Electron-impact ionization of all ionization stages of krypton

S. D. Loch and M. S. Pindzola
Department of Physics, Auburn University, Auburn, Alabama 36849

C. P. Ballance, D. C. Griffin, and D. M. Mitnik
Department of Physics, Rollins College, Winter Park, Florida 32789

N. R. Badnell, M. G. O'Mullane, H. P. Summers, and A. D. Whiteford
Department of Physics, University of Strathclyde, Glasgow G4 0NG, United Kingdom
(Received 12 July 2002; published 14 November 2002)

Configuration-average distorted-wave calculations are carried out for electron-impact single ionization of all ionization stages of krypton. Contributions to the cross sections are included from both direct ionization and excitation autoionization. Good agreement with experimental crossed-beams measurements is found for many of the moderately charged ionization stages. Maxwellian-averaged rate coefficients are calculated for each ionization stage and then archived for future use in studies of ionization balance in astrophysical and laboratory plasmas.

DOI: 10.1103/PhysRevA.66.052708 PACS number(s): 34.80.Dp, 52.20.Fs

I. INTRODUCTION

An important element in controlled fusion experiments is krypton, where it is used as an ion density diagnostic and is pumped into the divertor to assist in radiative cooling [1]. As a consequence, a great deal of theoretical and experimental work has been done on the study of electron-impact excitation and ionization of the krypton atom and its ions. In the following two paragraphs we review previous studies of the electron-impact single ionization of the krypton atom and its ions.

The electron-impact ionization cross section for the neutral krypton atom has been experimentally measured by several groups [2–4]. Ionization cross sections for Kr^{+}, Kr^{2+}, and Kr^{3+} were measured by Tinschert *et al.* [5] and checked against the parametric expression of Lotz [6]. Ionization cross sections for Kr^{4+}, Kr^{5+}, and Kr^{7+} were measured by Bannister *et al.* [7]. Gorczyca *et al.* [8] carried out configuration-average distorted-wave calculations for the ionization of Kr^{4+}, Kr^{5+}, Kr^{6+}, and Kr^{7+}, while also studying term-dependence and resonance-excitation effects within the distorted-wave and close-coupling approximations for Kr^{6+} and Kr^{7+}. Mitnik *et al.* [9] also carried out fully relativistic distorted-wave calculations for the ionization of Kr^{6+}. Ionization cross sections for Kr^{8+} were measured and compared with configuration-average distorted-wave calculations by Bannister *et al.* [10]. The Kr^{8+} measurements were strongly affected by ionization from metastable states in the first excited configuration. Ionization cross sections for Kr^{10+} and Kr^{11+} were measured by Oualim *et al.* [11] and compare well with the configuration-average distorted-wave calculations of Teng *et al.* [12].

Recently, ionization cross sections for Kr^{12+} through to Kr^{18+} were measured by Khouilid *et al.* [13] using an animated crossed-beams method. Only the Kr^{18+} measurements were compared with the configuration-average distorted-wave calculations, the rest only being checked against the Lotz parametric expression [6]. Although there are no experimental measurements for more highly charged ions than Kr^{18+}, there are a few theoretical studies. Chen and Reed [14] carried out fully relativistic distorted-wave calculations for the ionization of Kr^{24+} and Kr^{25+}, including contributions from both resonant excitation and excitation-autoionization. Badnell and Pindzola [15] carried out level to level distorted-wave calculations for the ionization of Kr^{30+}, Kr^{31+}, and Kr^{32+}, also including contributions from both resonant excitation and excitation autoionization.

In this paper we present a complete study of the electron-impact single ionization of the krypton atom and its ions, calculating configuration-average distorted-wave cross sections and rate coefficients for all ionization stages. Using modern scripting languages that manipulate both input and executable files, the calculation of direct and indirect contributions to the total ionization cross sections has been automated in preparation for large-scale calculations of all ionization stages of heavy elements [16]. In the light of current fusion experiments to investigate the use of heavy elements, such as tungsten, for use as wall erosion markers and wall surface components, there is a need for comprehensive atomic data for such complex species [17].

Because of its importance as a fusion plasma diagnostic, krypton was chosen to test the automated running of the configuration-average distorted-wave codes. As outlined in the previous paragraphs, there is a substantial amount of experimental measurements against which the configuration-average distorted-wave results can be checked. There are also recent experimental measurements that are yet to be compared with distorted-wave theory, i.e., Kr^{12+} through to Kr^{17+}. Many of the krypton cross sections have already been calculated using distorted-wave theory, and more complex techniques, so that only a small selection of the full results are presented. For the lower ionization stages of krypton, dominated by direct ionization, the configuration-average distorted-wave approach is the only currently feasable method of calculating ionization cross sections. The *R* matrix with pseudostates, convergent close coupling, and time-

dependent close-coupling methods have only been applied to calculate direct ionization cross sections for relatively simple ions involving one or two active electrons. For the moderately ionized stages of krypton, in which indirect ionization processes become more important, the standard *R* matrix and level-to-level multiconfiguration distorted-wave methods have been applied to calculate excitation-autoionization contributions. For the total indirect ionization cross section, the configuration average distorted-wave method can be just as accurate as these more complex methods. That is, a good total sum over the many terms or levels present in these complex systems is somewhat easier to obtain than any one individual term or level cross section. The configuration average distorted-wave approach also allows us to generate data for a complete isonuclear sequence for heavy elements such as krypton, something that would be impractical using more complex methods.

The direct and indirect contributions to the ionization cross section are integrated with a Maxwellian electron distribution to provide rate coefficients for plasma modeling. Both initial and final state level resolution for the configuration-average direct ionization rates is recovered exactly by simple multiplication by the appropriate angular branching factors [18]. Level resolution for the configuration-average indirect ionization rates is recovered only approximately by simple multiplication by the appropriate statistical weights. The configuration-average rate coefficients will be archived in the database for the Atomic Data and Analysis Structure (ADAS) Project [19,20] and will also be available on the Internet at the Oak Ridge National Laboratory's (ORNL) Controlled Fusion Atomic Data Center [21]. The final aim in the generation of such complex species data is the spectral modeling and fitting of heavy element spectra. This requires absolute excited-state populations. Thus, the rate coefficients generated in this paper will be used both in ionization balance calculations and in collisional-radiative modeling of excited-state populations. In Sec. II we give a brief review of the theoretical and computational methods, in Sec. III we compare our theoretical results against experiment and other calculations, while in Sec. IV we conclude with a brief summary.

II. THEORY

Major contributions to the electron-impact single-ionization cross section are made by the following two processes:

$$e^- + \mathrm{Kr}^{q+} \rightarrow \mathrm{Kr}^{(q+1)+} + e^- + e^-, \tag{1}$$

$$e^- + \mathrm{Kr}^{q+} \rightarrow (\mathrm{Kr}^{q+})^* + e^- \rightarrow \mathrm{Kr}^{(q+1)+} + e^- + e^-, \tag{2}$$

where q is the residual charge on the atom. The first process is termed direct ionization, and the second is excitation autoionization. For highly charged atoms, the radiative-stabilization process,

$$(\mathrm{Kr}^{q+})^* \rightarrow \mathrm{Kr}^{q+} + \gamma, \tag{3}$$

acts to reduce the contribution from excitation autoionization. An additional process,

$$e^- + \mathrm{Kr}^{q+} \rightarrow (\mathrm{Kr}^{(q-1)+})^{**} \rightarrow (\mathrm{Kr}^{q+})^* + e^- \rightarrow \mathrm{Kr}^{(q+1)+} + e^- + e^-, \tag{4}$$

called resonant-excitation double autoionization, may also contribute to the single ionization of an atom. Autoionization of $(\mathrm{Kr}^{(q-1)+})^{**}$ to a bound state of Kr^{q+}, or various radiative stabilization processes, acts to reduce the contribution from resonant-excitation double-autoionization.

For each ionization stage of krypton, a set of initial and final configurations are needed for each collisional ionization process. For example, the ground configuration of Kr^{25+}, $1s^2 2s^2 2p^6 3s$, is connected to the final ground configuration of Kr^{26+}, $1s^2 2s^2 2p^6$, giving direct ionization of the $3s$ subshell. Likewise, the initial ground configuration of Kr^{25+} is connected to the final excited configuration of Kr^{25+}, $1s^2 2s^2 2p^5 3s 3d$, giving excitation autoionization. For each ionization stage, the required sets of configurations are generated automatically via a code that is part of the ADAS suite of codes [20]. Using a graphical interface, one chooses the possible configurations for use in the ionization calculations via the entry of some boundary conditions (e.g., lowest nl subshell to directly ionize from, highest nl subshell to include in the excitation autoionization calculation). These boundary conditions are used to generate configuration lists for all ionization stages of interest. Some fine-tuning of this configuration list is possible, for example, for Kr^{4+} direct ionization from the $3d$ subshell is not calculated because the resulting Kr^{5+} configuration is autoionizing and thus contributes to the double ionization of Kr^{4+}. Thus, a refined configuration list for ionization was generated for all stages of krypton and the relevant driver files for the various atomic structure and electron-atom collision codes produced.

A modern scripting language is used to match driver files with and run the executables for the various structure and scattering codes. The threshold energies and the bound radial orbitals for the krypton configurations are calculated using the Hartree-Fock relativistic atomic structure code of Cowan [22], where the mass-velocity and Darwin terms are included in the radial Schrödinger equation. The direct and excitation-autoionization contributions to electron-impact single ionization of an atom or ion are calculated in a configuration-average distorted-wave approximation [23], which has been successfully employed in the study of many ionized systems [24–29]. The continuum radial orbitals are calculated as distorted-wave solutions of the radial Schrödinger equation using configuration-average Hartree and semiclassical exchange potentials and also including mass-velocity and Darwin terms. For the more highly charged ionization stages, configuration-average radiative and autoionization rates are evaluated and used to determine the branching ratios needed for contributions from excitation autoionization. In this work, we have not included contributions from resonant-excitation double autoionization, which are generally small compared to the contribution from excitation autoionization. The main limitation of the configuration-average approach is that it does not account for interaction among configurations.

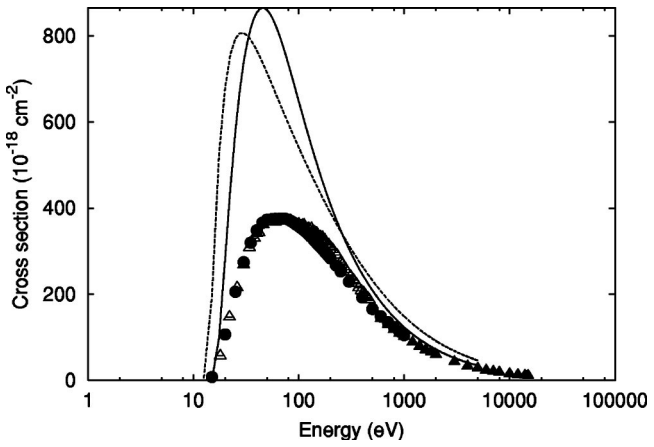

FIG. 1. Electron-impact single-ionization cross section of neutral Kr. Configuration-average distorted-wave results for the ground configuration, $3d^{10}4s^24p^6$, solid curve, prior form; dashed curve, post form. Experimental measurements; ● symbol [2], △ symbol [3], ▲ symbol [4]. Note that the experimental error bars are too small to be seen on the graph.

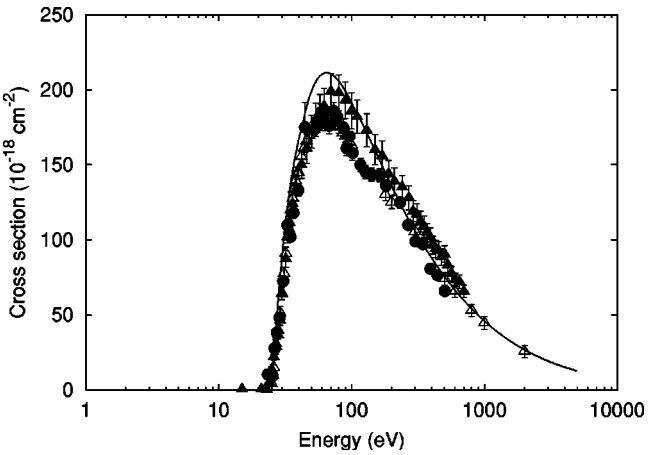

FIG. 2. Electron-impact single-ionization cross section of Kr^+. Configuration-average distorted-wave results for the ground configuration, $3d^{10}4s^24p^5$, are given by the solid curve. Experimental measurements; ● symbol [37], △ symbol [36], ▲ symbol [5].

The ionization cross sections are transformed into rate coefficients by integration with a Maxwellian velocity distribution at the appropriate temperature. The calculated ionization cross sections are fitted to simple functions of the incident electron energy to provide parameters for the Maxwellian integration. Configuration-average photoionization calculations are used to obtain the infinite energy limit point for the direct contributions to electron-impact ionization. The cross section contributions from excitation autoionization at the higher incident energies are given by extrapolations of fits to the lower-energy results. The resultant rate coefficients are archived in an ADAS standard data format on a 12 point temperature grid.

III. RESULTS

A. Single ionization of the neutral Kr atom

Configuration-average distorted-wave results for the electron-impact single ionization of neutral krypton are presented in Fig. 1. A comparison with the experimental measurements of various authors [2–4] is shown. In the running of the configuration-average distorted-wave codes one can select either a post or prior form for the first-order scattering amplitude. The prior form means that the incident and scattered electrons are calculated in a V^N potential, while the bound and ejected electrons are calculated in a V^{N-1} potential (N being the number of bound electrons on the target ion). In the post form for the scattering amplitude all electrons experience a V^{N-1} potential. Both the post and prior results for neutral krypton are shown in Fig. 1. The prior form produces better high-energy results, but neither can reproduce either the height or shape of the experimental cross section for neutral Kr. It has been found that the prior form can lead to nonphysical shape resonances for neutral species [30], so it was decided to use the post form in all future calculations of neutral atoms. The post and prior forms produce very similar results for ionization of positively charged atomic ions. For more accurate neutral atom ionization cross sections one should use various nonperturbative methods, such as the R matrix with pseudostates [31], convergent close coupling [32], time-dependent close coupling [33], hyperspherical close-coupling [34], or exterior complex scaling methods [35].

B. Single ionization of moderately charged Kr ions

As the residual ion charge increases, the perturbative distorted-wave method has been found to become more accurate. There is also a general trend with increasing ion charge whereby the ionization threshold energy increases and the peak cross section value decreases. At certain ionization stages, the excitation-autoionization contribution to the cross section becomes significant. This occurs primarily when a nearly empty subshell sits above a full subshell. For example, we expect that electron-impact ionization from the ground $3d^{10}4s$ configuration of Kr^{7+} and the ground $2p^63s$ configuration of Kr^{25+} would have large contributions from excitation autoionization.

Configuration-average distorted-wave results for the electron-impact single ionization of Kr^+ are presented in Fig. 2, where they are compared with experimental measurements [5,36,37]. We note that the contributions from excitation autoionization are small, and that the theoretical results are slightly higher than most of the experimental measurements. As has been seen in previous studies of electron-impact ionization of elements along their iso-nuclear sequences, there is a great improvement in the configuration-average distorted-wave results for the singly ionized case.

Configuration-average distorted-wave results for the electron-impact single ionization of Kr^{2+} are presented in Fig. 3, where they are compared with experimental measurements of Man *et al.* [38]. At the peak of the ionization cross section, theory and experiment are in excellent agreement.

Configuration-average distorted-wave results for Kr^{3+} ionization are presented in Fig. 4, along with the experimental measurements of Tinschert *et al.* [5] and Gregory *et al.*

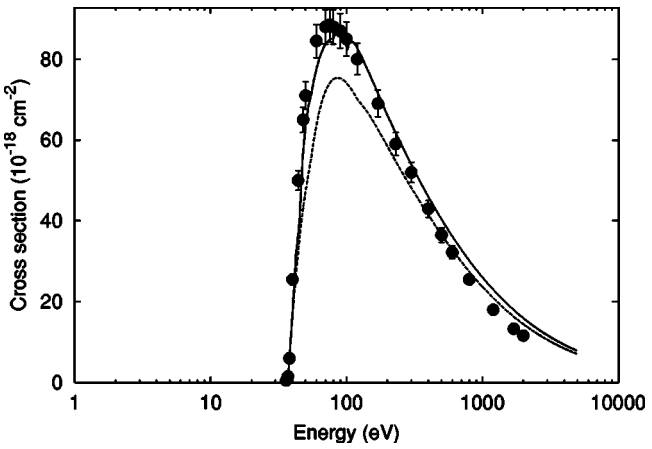

FIG. 3. Electron-impact single-ionization cross section of Kr^{2+}. Configuration-average distorted-wave results for the ground configuration, $3d^{10}4s^24p^4$, solid curve, total cross section; dashed curve, direct cross section only. Experimental measurements; ● symbol [38].

[39]. We note that there is no direct ionization contribution from the $3d$ subshell, $3d$ ionization instead contributes to the double ionization of Kr^{3+}. Our results are in closer agreement with the experimental results of Gregory *et al.* [39] than those of Tinschert *et al.* [5]. In the Tinschert *et al.* measurements [5] the presence of a small amount of ionization cross section below the theoretical ground configuration ionization threshold suggests the presence of metastable states in their beam. Configuration-average distorted-wave cross sections were generated for ionization from the excited configuration $3d^{10}4s^24p^24d$. We found that the onset of the ionization cross section was lower than experiment, and that the peak cross section was higher than experiment. Thus, the presence of a small fraction of metastable states in the beam may explain the differences between the configuration-average distorted-wave results and the experimental results. Our configuration-average distorted-wave results for Kr^{4+}

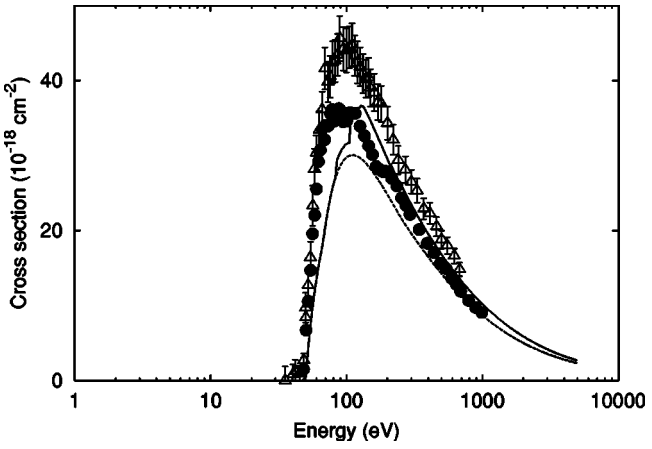

FIG. 4. Electron-impact single-ionization cross section of Kr^{3+}. Configuration-average distorted-wave results for the ground configuration, $3d^{10}4s^24p^3$, are shown for the total cross section by the solid line and for the direct cross section by the dashed line. Experimental measurements; △ symbol [5], ● symbol [39].

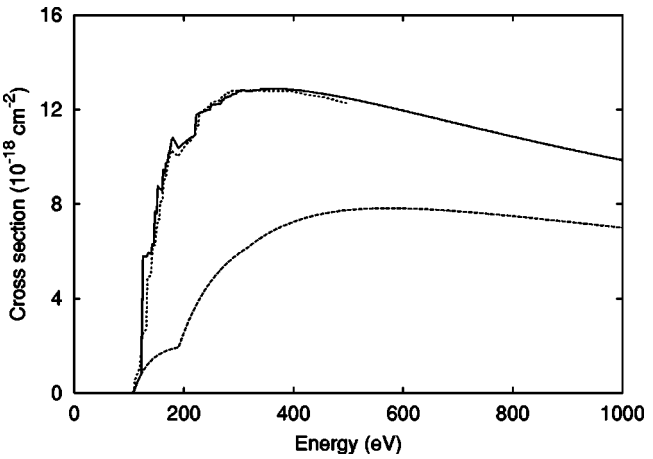

FIG. 5. Electron-impact single-ionization cross section for the ground configuration, $3d^{10}4s^2$, of Kr^{6+}. Configuration-average distorted-wave results, solid curve, total cross section; long-dashed curve, direct cross section only. Relativistic distorted-wave results [9] for the total cross section are given by the short-dashed curve.

through to Kr^{7+} are found to be in reasonable agreement with those calculated previously by Gorczyca *et al.* [8]. In Fig. 5 we compare our configuration-average distorted-wave results for Kr^{6+} with the level resolved relativistic distorted-wave results of Mitnik *et al.* [9]. We note that excitation-autoionization contributions are large for ionization from the ground $3d^{10}4s^2$ configuration of Kr^{6+}, and that there is excellent agreement between the two theoretical results. It should be noted that the results of Gorczyca *et al.* [8] are preferred over the configuration-average distorted-wave re-

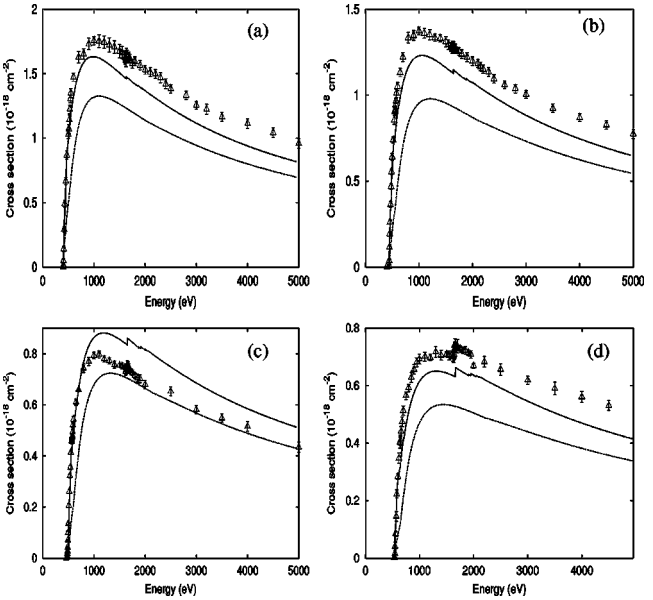

FIG. 6. Configuration-average distorted-wave single-ionization cross section for the following ground configurations: (a) $3s^23p^63d^6$ of Kr^{12+}, (b) $3s^23p^63d^5$ of Kr^{13+}, (c) $3s^23p^63d^4$ of Kr^{14+}, and (d) $3s^23p^63d^3$ of Kr^{15+}. In all plots the long dashed curves are for the total configuration-average distorted-wave results and the short-dashed curve represents the direct cross section. Experimental measurements; △ symbol [13].

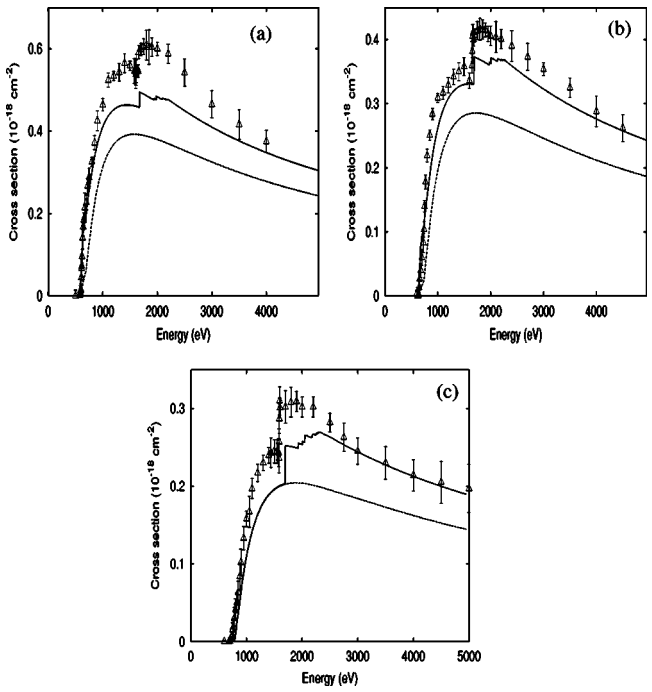

FIG. 7. Configuration-average distorted-wave single-ionization cross section for the the following ground configurations: (a) $3s^2 3p^6 3d^2$ of Kr^{16+}, (b) $3s^2 3p^6 3d$ of Kr^{17+}, and (c) $3s^2 3p^6$ of Kr^{18+}. In all plots the long-dashed curves are the total configuration-average distorted-wave results and the short-dashed curve represents direct cross section. Experimental measurements; $\triangle$ symbol [13].

sults for Kr^{6+} and Kr^{7+}, as one needs to include term dependence and relaxation of the $3d$ orbital to obtain the best agreement with experiment near threshold.

Our configuration-average distorted-wave results for Kr^{10+} and Kr^{11+} are found to be in excellent agreement with the experimental measurements of Oualim *et al.* [11]. They are also in excellent agreement with similar distorted-wave calculations of Teng *et al.* [12].

Configuration-average distorted-wave results for the electron-impact single ionization of Kr^{12+}, Kr^{13+}, Kr^{14+}, and Kr^{15+} are presented in Fig. 6, while results for Kr^{16+}, Kr^{17+}, and Kr^{18+} are presented in Fig. 7. In both Figs. 6 and 7, theory is compared with the recent experimental measurements of Khouilid *et al.* [13]. Reasonable agreement between theory and experiment is found for all of these ionization stages. As can be seen from Figs. 6 and 7 the contributions from excitation autoionization become more important as the $3d$ subshell becomes less occupied. For Kr^{16+}, Kr^{17+}, and Kr^{18+} the $2p$ direct ionization contributes to the double ionization of those stages.

There are some inherent uncertainties in both the configuration-average distorted-wave calculations and in the experimental measurements for these stages which may explain the differences in the results. For highly ionized stages such as Kr^{12+} through to Kr^{18+}, one expects the configuration-average distorted-wave direct ionization cross sections to be quite accurate. The main difficulty with the theory for these stages is that some excited configurations lie close to the ionization thresholds for each ion. Level splitting of these excited configurations can straddle the levels over the ionization threshold, potentially increasing or decreasing the excitation autoionization cross section depending upon whether the configuration average excited energy lies above or below the threshold. It should be noted that there are also some difficulties with the experimental measurement of such highly ionized stages. The ionization cross sections for these stages are small, and are subsequently difficult to measure. It is also difficult to obtain pure ground configurations in the experimental beam, and the presence of metastable states in the beam can significantly alter the cross section. This is, in fact, an issue with some of these stages, Khouilid *et al.* [13] reported the presence of metastable states in their ion beam for Kr^{14+}, Kr^{16+}, and Kr^{18+}. For Kr^{14+} and Kr^{16+} the reported metastable states are found in the ground configurations, while for Kr^{18+} the metastable states were found in the first excited configuration.

We find good agreement above threshold between the Kr^{18+} cross sections and our configuration-average calculation from the ground configuration, however, there is a small amount of measured ionization cross section below the configuration-average threshold. We calculated the ionization cross section for the excited configuration $3s^2 3p^5 3d$ of Kr^{18+} and found that the ionization threshold was slightly below the experimentally measured threshold and that the peak cross section was above that of the experiment. Thus, the presence of a small fraction of metastable states in the beam may explain the differences between the configuration-average distorted-wave calculations for the ground configuration and the experimental cross section.

C. Single ionization of highly charged Kr ions

As krypton becomes more highly ionized, radiative stabilization competes with the autoionization rate and the autoionization branching ratio becomes smaller than 1. Thus, for the more highly ionized stages, configuration-average branching ratios were calculated and were found to differ significantly from 1 for Kr^{19+} through to Kr^{25+}. As an example, we show the results for Kr^{24+} and Kr^{25+} in Figs. 8 and 9. It can be seen that, as expected, the inclusion of branching ratios significantly reduces the distorted-wave cross sections. The resultant cross sections are in good agreement with those calculated by Chen and Reed [14].

For the more highly ionized stages of Kr the ionization threshold continues to increase with charge state and the height of the cross section continues to decrease. For all ionization stages above Kr^{25+}, contributions from excitation autoionization are small compared to the direct contributions, as was seen in the work of Badnell and Pindzola [15] for Kr^{30+}, Kr^{31+}, and Kr^{32+}.

D. Rate coefficients for Kr ions

Direct and indirect ionization cross sections are integrated with a Maxwellian electron velocity distribution to produce rate coefficients. As an example, we present direct ionization rate coefficient results for the 1s orbital of Kr^{33+} in Fig. 10. The top curve shows the configuration-average rate for the

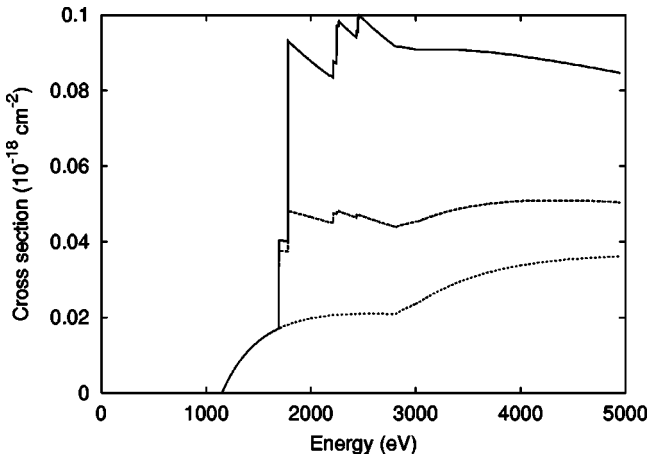

FIG. 8. Configuration-average distorted-wave single-ionization cross section results for the ground configuration $3s^2$ of Kr^{24+}. Solid line, without branching ratios; long-dashed line, with branching ratios; short-dashed line, direct cross section only.

$1s^22s \rightarrow 1s2s$ transition. In order to compare with the first-order relativistic perturbation calculation of Sampson and Zhang [40] we multiply the configuration-average results by the appropriate angular branching factors to get level resolved direct ionization rates of the 1s orbital. The factor is 0.75 for $1s^22s\,^2S_0 \rightarrow 1s2s\,^3S_1$ and 0.25 for $1s^22s\,^2S_0 \rightarrow 1s2s\,^1S_0$. It can be seen from Fig. 10 that there is good agreement between our results and those of Sampson and Zhang [40].

The krypton ionization data that are stored in the ORNL database are at configuration-average resolution. The ionization rate coefficients are archived on a reduced temperature grid spanning from 2×10^2 K through to 2×10^6 K. The rates are from the ground configurations, with direct ionization from the four outer subshells (provided they do not contribute to the double ionization of the ion), and indirect ionization from the three subshells below the valence shell. For the indirect rates, the configuration-average rates are stored

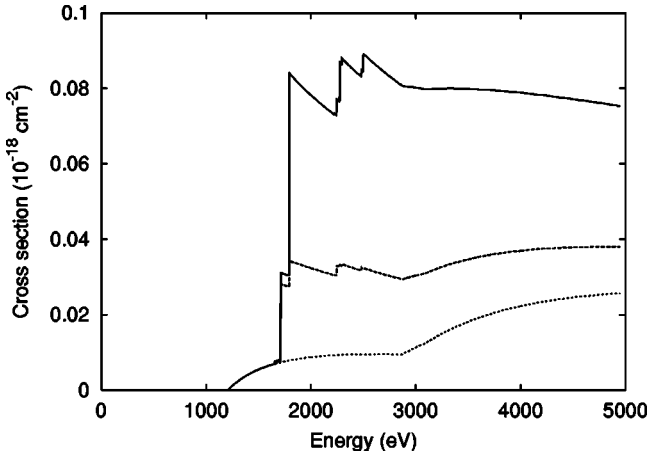

FIG. 9. Configuration-average distorted-wave single-ionization cross section results for the ground configuration $3s$ of Kr^{25+}. Solid line, without branching ratios; long-dashed line, with branching ratios; short-dashed line, direct cross section only.

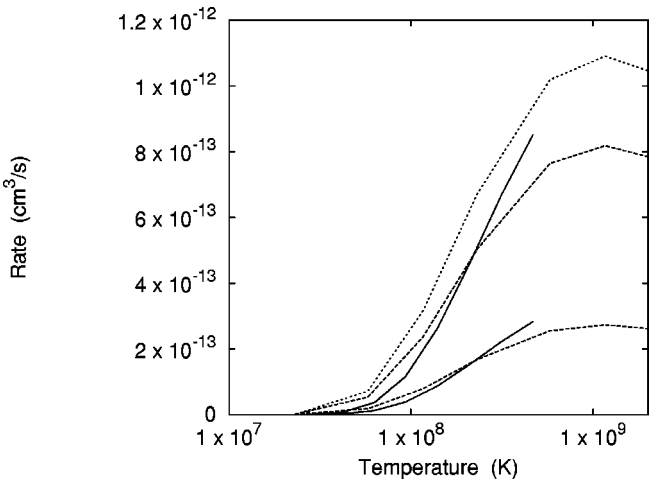

FIG. 10. Single-ionization rate coefficient from the ground state $1s^22s\,^1S_0$ of Kr^{33+}. Top line is the configuration-average rate coefficient. Of the lower sets of lines the upper lines show ionization to $1s2s\,^3S_1$ (solid line, results of Ref. [40], long-dashed line, configuration-average disorted-wave results). Lower lines, ionization to $1s2s\,^1S_0$ (solid line, results of Ref. [40], long-dashed line, configuration-average distorted-wave results).

for each excited nl subshell that is autoionizing. These configuration-average datafiles may be transformed into stage to stage ionization rates, giving the total ionization rate from one ionization stage to the next stage.

The configuration-average datafiles can also be transformed into level resolved data files (referred to as ADAS adf23 files [20]). The direct ionization rates are produced using angular branching factors as described above for the case of Kr^{33+}. The indirect ionization rates can be transformed into level resolved rates using a statistical approximation. As in the configuration-average case, the level resolved excitation-autoionization rates would be stored for each excited nl subshell that can autoionize. Note that we archive the configuration-average datafiles, along with the energy-level information and cross-section fitting coefficients required to process the files into level resolved datafiles.

IV. SUMMARY

Electron-impact single-ionization cross sections were calculated in the configuration-average distorted-wave approximation for the complete ionization sequence of krypton. Direct ionization, excitation autoionization, and autoionizing branching ratios were all accounted for. For neutral Kr the configuration-average distorted-wave results were higher than experiment. For many of the moderately charged ionization stages good agreement with crossed-beams experimental measurements was found. In particular, the configuration-average distorted-wave results for Kr^{12+} through to Kr^{17+} were in reasonable agreement with experiment and are the first distorted-wave calculations to be compared with experiment for those stages. For the more highly ionized stages autoionization branching ratios were calculated, and were found to decrease the excitation-autoionization contributions for Kr^{19+} through to Kr^{25+}.

Configuration-average direct and indirect rate coefficients were calculated for all ionization stages of krypton and archived in the ADAS database and at the ORNL website. The direct ionization rate coefficient can be accurately transformed into level resolved rates. The indirect rate coefficient may be transformed into level resolved rates using a statistical approximation. The computer codes used to generate the ionization cross sections and rate coefficients can be run for any isonuclear sequence with minimal user interaction and are intended for use in generating ionization data for analysis of heavy element wall erosion studies for fusion.

ACKNOWLEDGMENTS

This work was supported in part by a U.S. Department of Energy SciDAC grant (Grant No. DE-FG02-01ER54644) to Auburn University. Much of the experimental data were obtained from the NIFS atomic database [41].

[1] M. L. Watkins *et al.*, JET Report No. JET-C(98)74, 1998 (unpublished).
[2] E. Krishnakumar and S. K. Srivastava, J. Phys. B **21**, 1055 (1988).
[3] J. A. Syage, Phys. Rev. A **46**, 5666 (1992).
[4] B. L. Schram, Physica **32**, 197 (1966).
[5] K. Tinschert, A. Muller, G. Hofmann, K. Huber, R. Becker, D. C. Gregory, and E. Salzborn, J. Phys. B **20**, 1121 (1987).
[6] W. Lotz, Z. Phys. **216**, 241 (1968).
[7] M. E. Bannister, X. Q. Guo, and T. M. Kojima, Phys. Rev. A **49**, 4676 (1994).
[8] T. W. Gorczyca, M. S. Pindzola, N. R. Badnell, and D. C. Griffin, Phys. Rev. A **49**, 4682 (1994).
[9] D. Mitnik, P. Mandelbaum, J. L. Schwob, A. Bar-Shalom, and J. Oreg, Phys. Rev. A **55**, 307 (1997).
[10] M. E. Bannister, D. W. Mueller, L. J. Wang, M. S. Pindzola, D. C. Griffin, and D. C. Gregory, Phys. Rev. A **38**, 38 (1988).
[11] E. M. Oualim, M. Duponchelle, and P. Defrance, Nucl. Instrum. Methods Phys. Res. B **98**, 150 (1995).
[12] H. Teng, P. Defrance, C. Cheg, and Y. Wang, J. Phys. B **33**, 463 (2000).
[13] M. Khouilid, S. Cherkani-Hassani, S. Rachafi, H. Teng, and P. Defrance, J. Phys. B **34**, 1727 (2001).
[14] M. H. Chen and K. J. Reed, Phys. Rev. A **47**, 1874 (1993).
[15] N. R. Badnell and M. S. Pindzola, Phys. Rev. A **47**, 2937 (1993).
[16] S. D. Loch, M. G. O'Mullane, H. P. Summers, and A. D. Whiteford, UKAEA Contract Report No. QS06915, 2002 (unpublished).
[17] G. F. Counsell, EU task No:DV7A-T438, 1999 (unpublished).
[18] D. H. Sampson, Phys. Rev. A **34**, 986 (1986).
[19] H. P. Summers, JET Joint undertaking Report No. JET-IR(93)07, 1993 (unpublished).
[20] H. P. Summers, ADAS Manual V2.5, http://adas.phys.strath.ac.uk/ (2002).
[21] http://www-cfadc.phy.ornl.gov/data_and_codes
[22] R. D. Cowan, *The Theory of Atomic Structure and Spectra* (University of California Press, Berkeley, 1981).
[23] M. S. Pindzola, D. C. Griffin, and C. Bottcher, in *Atomic Processes in Electron-ion and Ion-ion Collisions, Vol. 145* of *NATO Advanced Study Institute, Series B: Physics*, edited by F. Brouillard (Plenum, New York, 1986), p. 75.
[24] M. S. Pindzola, D. C. Griffin, C. Bottcher, S. M. Younger, and H. T. Hunter, Oak Ridge National Laboratory Report No. ORNL/TM-10297, 1987 (unpublished).
[25] M. S. Pindzola, D. C. Griffin, C. Bottcher, M. J. Buie, and D. C. Gregory, Phys. Scr. T **37**, 35 (1991).
[26] D. Hathiramani, K. Aichele, G. Hofmann, M. Steidl, M. Stenke, R. Volpel, and E. Salzborn, M. S. Pindzola, J. A. Shaw, D. C. Griffin, and N. R. Badnell, Phys. Rev. A **54**, 587 (1996).
[27] J. Colgan, D. M. Mitnik, and M. S. Pindzola, Phys. Rev. A **63**, 012712 (2001).
[28] J. A. Shaw, M. S. Pindzola, M. Steidl, K. Aichele, U. Hartenfeller, D. Hathiramani, F. Scheuermann, M. Westermann, and E. Salzborn, Phys. Rev. A **63**, 032709 (2001).
[29] K. Aichele, W. Arnold, D. Hathiramani, F. Scheuermann, E. Salzborn, D. M. Mitnik, D. C. Griffin, J. Colgan, and M. S. Pindzola, Phys. Rev. A **64**, 052706 (2001).
[30] M. S. Pindzola, D. C. Griffin, and J. H. Macek, Phys. Rev. A **51**, 2186 (1995).
[31] K. Bartschat and I. Bray, J. Phys. B **29**, L577 (1996).
[32] I. Bray and A. T. Stelbovics, Phys. Rev. Lett. **70**, 746 (1993).
[33] M. S. Pindzola and F. Robicheaux, Phys. Rev. A **54**, 2142 (1996).
[34] D. Kato and S. Watanabe, Phys. Rev. Lett. **74**, 2443 (1995).
[35] M. Baertschy, T. N. Rescigno, W. A. Isaacs, X. Li, and C. W. McCurdy, Phys. Rev. A **63**, 022712 (2001).
[36] K. F. Man, A. C. H. Smith, and M. F. A. Harrison, J. Phys. B **20**, 5865 (1987).
[37] H. Gao, D. Fang, F. Lu, J. Gu, W. Wu, W. Hu, Y. Wang, S. Wu, J. Tang, and F. Yang, Nucl. Instrum. Methods Phys. Res. B **132**, 364 (1997).
[38] K. F. Man, A. C. H. Smith, and M. F. A. Harrison, J. Phys. B **26**, 1365 (1993).
[39] D. C. Gregory, P. F. Dittner, and D. H. Crandall, Phys. Rev. A **27**, 724 (1983).
[40] D. H. Sampson and H. L. Zhang, Phys. Rev. A **37**, 3765 (1988).
[41] NIFS Atomic and Molecular database, http://dbshino.nifs.ac.jp